ISSN 1023-1935, Russian Journal of Electrochemistry, 2024, Vol. 60, No. 3, pp. 216–222. © Pleiades Publishing, Ltd., 2024.

Calcium–Borosilicate Glass-Ceramics as a Sealant for Solid Oxide Fuel Cells[1]

A. O. Zhigachev[a], *, S. I. Bredikhin[a], E. A. Agarkova[a], **, and D. V. Matveev[a]

[a] *Osipyan Institute of Solid State Physics RAS, Chernogolovka, Russia*

**e-mail: zhigachev@issp.ac.ru*

***e-mail: stepanova.ea@issp.ac.ru*

Received September 23, 2022; revised August 29, 2023; accepted September 28, 2023

Abstract—The applicability of calcium–borosilicate glass-ceramics with high boron oxide content as a sealant for solid oxide fuel cells is studied. Chemical composition of the studied materials is: 33 mol % CaO, 21 mol % B_2O_3, and 46 mol % SiO_2. The material is studied as an alternative to the existing calcium– and barium–aluminosilicate-based sealants because of the latters' limited adhesion to steel interconnects in fuel cells. The studied sealant is shown to have a softening point of about 920–930°C, which allows using it for sealing of fuel cells at 925°C. Use of relatively low sealing temperature allows avoiding overheating of the cell during the sealing and avoiding the accompanying degradation of the battery operational characteristics. The studied sealant demonstrated excellent adhesion to the surface of interconnect materials (the Crofer 22 APU steel). Furthermore, the studied sealant is found to be thermomechanically compatible with the Crofer 22 APU steel and ZrO_2-based electrolytes.

Keywords: SOFC, glass-ceramics, crystallization, sealing

DOI: 10.1134/S1023193524030121

INTRODUCTION

The solid oxide fuel cells (SOFC) are the perspective electrochemical devices converting the chemical energy of hydrogen and hydrocarbon fuel to the electrical energy. The process of energy conversion occurs directly via electrochemical reactions, by-passing the fuel combustion stage. The SOFC compatibility with the hydrocarbon fuel together with its high efficiency and practically silent operation made it attractive for the energy industrial generation [1].

The SOFCs are compatible with the hydrocarbon fuel thanks to their high operation temperature, because the majority of commercial SOFC have the operation temperature of 800–1000°C. Notably, an activity in the development of the SOFC working at medium (600–800°C) and lower temperatures (500–600°C) has been indicated in the recent two decades [2, 3], although such plants have not yet reached the industrial application. Unfortunately, the higher operation temperatures have disadvantages as well: they posed more requirements to the thermomechanical and chemical compatibility of the SOFC materials, in particular, complicated the sealant selection.

Sealants in the SOFC separate the fuel and air flows, isolate inner gas flows from the environment, and provide the battery mechanical integrity [1]. The SOFC sealants used to be glasses and glass-ceramics. The sealant selection for SOFC is a challenging task because the sealant must meet quite a number of requirements. The basic requirement is: the sealant must be thermomechanically compatible with electrolyte and the bipolar plate material (the latter usually is a refractory chrome steel), that is, it must have the coefficient of temperature expansion (CTE) falling into the $(8–12) \times 10^{-6}$ 1/K range [4–6]. The second requirement is the sealant strong adhesion to the steel surface [4]. It is essential to the battery strong mechanical integrity and the absence of gas leakages through the insecure interface. In addition, the sealant properties must not change significantly as the SOFC operates, due to, e.g., crystallization processes or chemical reactions.

Nowadays, the most popular SOFC sealants are:

(1) Barium–aluminosilicate-based glass-ceramics. Their composition often approaches the following: 45–55 mol % SiO_2, 5–15 mol % B_2O_3, 20–30 mol % BaO, 5–15 mol % Al_2O_3, with minor impurities of other oxides. These materials have an CTE of $(10.5–11) \times 10^{-6}$ 1/K, approaching that of zirconia and ceria electrolytes. They have a good adhesion to refractory steels, e.g., Crofer 22 APU [7–13].

[1] Based on the paper presented at the IX All-Russia Conference with international participation "Fuel Cells and Power Plants Based on Them," Chernogolovka, Moscow region, Russia, 2022.

(2) Diopside-based glass-ceramics $CaMg(Si_2O_6)$. Their exemplary chemical formula is: 15–20 mol % CaO, 25–35 mol % MgO, 45–50 mol % SiO_2, and minor admixtures of Al_2O_3, SiO_2, and B_2O_3 [9, 14, 15]. These sealants have a CTE about 10×10^{-6} 1/K and a good adhesion to the Crofer 22 APU.

(3) Modified sodium–lime silicate glass; the modification involves an increase of the CaO fraction and adding of alumina. It may be thought of as a sealant for the SOFC [7].

The above-listed materials, the more so, the barium–aluminosilicate-based glass-ceramics provided the SOFC hermitization and rather strong interconnecting of neighboring elements in the batteries. However, the very process of the SOFC hermitization with these materials involves the heating of the entire battery up to a temperature by 100–150°C higher than the battery working temperature. For example, the sealing of the battery operating at 850°C is carried out at 950°C (with a Schott G018-394 glass). The exposure to the elevated temperature used lasting several hours, it is necessary for the formation of reaction layer at the sealant/steel interface in order to provide the proper adhesion. The long exposure to elevated temperature can lead to changes in the electrode structure and thermomechanical strains in zones of dissimilar materials' contact [16], thus deteriorating the battery's operational characteristics. Hence, the desirable sealant is the one easily reacting with the bipolar-plate material, thus forming a strong interface remaining stable at the battery's operational temperature [4].

In this work, we studied a $CaO–SiO_2–B_2O_3$ sealant with high boron oxide content (21 mol %). We chose the system basing on the literature data which pointed that the boron-silicate glass with high boron oxide content has the CTE falling into the $(8–10) \times 10^{-6}$ 1/K range, the glass transition point about 650–700°C, and the softening temperature approaching 900–1000°C [16–19]. The basic aim of the study is the investigation of the $CaO–SiO_2–B_2O_3$ sealant adhesion to the Crofer 22 APU refractory steel under the conditions of short-time sealing (thermal treatment) at the lower temperatures than used to apply for the commercial sealants. In addition, we evaluated its post-treatment thermomechanical compatibility with the Crofer 22 APU steel.

Nowadays, the $CaO–SiO_2–B_2O_3$-system sealants are not used in the SOFC; yet, they find immediate application in the hermitization of the microelectronics' components operating at the near-room temperature [20–22]. The application of these sealants at higher temperatures is limited by the boron oxide volatility in amorphous compounds, leading to the cathode material poisoning [23, 24]. However, in this work, we hope lowering the boron oxide volatility by the reaching of the sealant higher crystallinity and its reacting with the steel, with the formation of the compounds binding the boron oxide.

EXPERIMENTAL

We prepared the sealant containing 33 mol % CaO, 21 mol % B_2O_3, and 46 mol % SiO_2. The choice of the composition is based on the recent publications on the application of calcium–borosilicate-based glasses [20–22]. As the starting materials for the sealant preparation, we used calcium carbonate, boric acid, and silica. All the chemicals (Khemkraft, Russia) had purity no less than 99%. To homogeneously mix the starting components, we added twice distilled water and agitated using a laboratory mixer for 5 min, then kept in drying oven at 100°C for 15 h, up to the water entire removal.

The dried mass was placed into platinum crucible and heated in air to 1500°C at a heating rate of 2.5°C/min. This low heating rate was chosen in order to prevent the substances' possible sputtering. The melt was kept at 1500°C for 1 h, to homogenize it, then quenched in twice distilled water.

The sealant dried particles were crushed in a mechanical mill (Fritsch Pulverisette 2), using a ZrO_2-mortar and pestle, to minimize the material pollution during the grinding. The fresh-prepared sealant was subjected to X-ray diffraction analysis (XRD), as well as that right after the thermal treatment as a pure material and in contact with the Crofer 22 APU alloy. The XRD was used for the determination of the crystal phases' presence and their composition. The XRD was performed using a SmartLab SE diffractometer (Rigaku, Japan) with copper anode.

To study the sealant high-temperature behavior, we hilled its small amount onto a Crofer 22 APU plate sized $20 \times 20 \times 2$ mm. The sealant powder made a hillock, about 10 mm in diameter, 10 mm in height. The plate with the powder was put to an oven and heated up to 850–975°C at a rate of 2°C/min, kept there for 1 h, and cooled at the same rate. The heating and cooling low rates were chosen to lower thermomechanical strains during the heating and cooling. The chosen heating rates approached those often used in the SOFC hermitization. After the high-temperature treatment, the sealant was crushed into fine powder, then its composition was studied using the XRD. Of the baked sealant, small stubs were cut off; the material CTE was measured in air by using a dilatometer. The sample heating and cooling rates were 3°C/min; the dilatometer baseline was measured witht an alumina standard sample. In the CTE measurements, we used a L75 Vertical dilatometer (LINSEIS, Germany).

Additionally, we studied the microstructure of the sealant/steel interface. To this purpose, we deposited the sealant onto a Crofer 22 APU plate; a F4200N benchtop robot (Fisnar, Denmark) was used in the deposition. The fresh-deposited sealant was dried, then covered by an identical Crofer 22 APU steel plate. The obtained structure was then loaded by the 1 N force and heated in an oven by the above-described

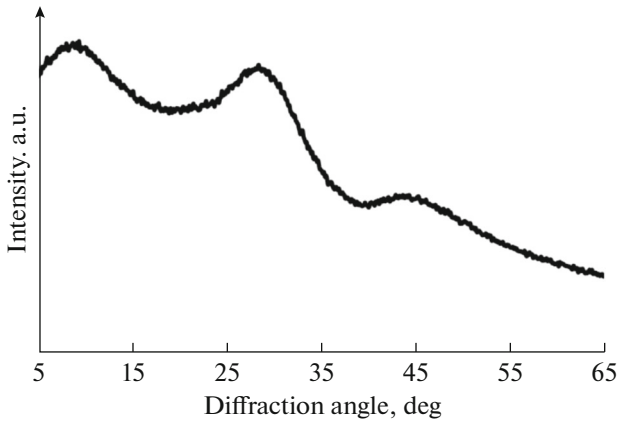

Fig. 1. XRD diffraction pattern of as-quenched $CaO–SiO_2–B_2O_3$ sealant.

protocol up to 850–975°C. In the plate center, a 150 μm-thick ZrO_2-restrictor was arranged, in order to obtain layer of the preset thickness. After the cooling, we made a cross-section of the joint, polished it, and obtained a SEM-image using a Supra 50VP scanning electron microscope (Carl Zeiss, Germany). The elemental analysis of the cross-section was carried out by the energy-dispersive X-ray analysis (EDX) method, using an INCA adapter (Oxford Instruments, UK) built-in to the scanning electron microscope.

RESULTS AND DISCUSSION

In Fig. 1 we show X-ray diffraction patterns of the crushed $CaO–SiO_2–B_2O_3$ sealant. The material showed no crystal peaks, only the amorphous-structure halo instead. In left to right order, they corresponded to interatomic distances of 9.251, 3.138, and 2.017 Å. Among them, only the 2.017 Å distance can be unambiguously counterposed to the B–O bond length [25]. Other ones can be counterposed either to the Si–O or Ca–O bonds whose lengths are 1.60–1.65 Å and 2.45–2.54 Å, respectively [26–28]. They may correspond to the distances between the glass neighboring ligaments, rather than that between the neighboring atoms.

To evaluate the wettability of the bipolar plate and electrolyte material surfaces by the sealant studied, we determined geometrical parameters of the sealant drop from the joint photographs, in particular, those taken with optical microscope. The photographs were taken in the plane perpendicular to the steel plate (or electrolyte) plane. The $CaO–SiO_2–B_2O_3$ sealant exposure at 850°C for 1 h caused no visible changes in the powder geometry. The increase in temperature up to 875°C lead to the powder angularity flattening and formation of a thin (~100 μm) dark-blue film. At 950°C the hillock relief is levelled off and the dark-blue film thickness increased to ~300 μm. At this temperature the sealant surface became smooth, and a droplet as if wetted out the steel surface, which can be controlled by the wetting angle. For the samples heated to 975°C we observed the sealant spreading out over the plate, which demonstrated the excellent steel wettability and the sealant low viscosity. Upon the reaching of the temperature of 900°C, a thin blue layer formed at the metal/sealant interface. This layer is likely to contain the products of the bipolar plate material reaction with the sealant. At the solid electrolyte (ZrO_2)/sealant interface we did not observe any colored reaction layer.

The experiments with the Schott 394 glass powder were carried out only at 950°C because it is the sealing temperature recommended by the manufacturer. The sealant softening degree at this temperature resembled that of $CaO–SiO_2–B_2O_3$ at 875°C. A significant difference was observed in the color of the sealant/steel contact surface: it was saturated-yellow, rather than the dark-blue one characteristic of the $CaO–SiO_2–B_2O_3$ mixture.

In Table 1 we give geometrical characteristics of the sealant droplets at the Crofer 22 APU-steel and ZrO_2-based solid electrolyte surfaces. To make the obtained geometrical characteristics more informative, we used the sealant aliquots identical in their mass and form.

We see from the table that the $CaO–SiO_2–B_2O_3$ sealant wetted perfectly the steel surface at all studied temperatures; at 950°C, the sealant surface spreading occurs—an adverse effect because it can deteriorate the sealant layer denseness and, correspondingly, the hermiticity. We also observed a good wettability of the solid electrolyte surface by the studied sealant.

The white and blue areas in the sealant were studied using the X-ray diffraction analysis after their thermal treatment at 950°C. They are the unreacted-sealant zones and the zone of the sealant reaction with the steel. In Fig. 2 we give X-ray diffraction patterns of the above-listed areas.

The sealant non-contacting the steel plate has fully crystallized (the lower curve in Fig. 2). The peaks in the X-ray diffraction patterns corresponded to CaB_2O_4, SiO_2 (crystobalite), and $CaSiO_3$. The amount of amorphous phase in the nonreacted sealant zone is negligibly small. The area ratio of the crystalline peaks of different phases allowed evaluating the content of different elements in the post-thermal-treated sealant: it approached the calculated amount (the deviation is <5%). The X-ray diffraction analysis of the reaction zone showed the presence of the same crystalline phases with similar molar composition, only the $CaSiO_3$ peaks appeared being somewhat more intense as compared with those of CaB_2O_4. This may be an indication that the boron oxide is partly involved in the reaction with the steel plate, without the calcium borate formation. The reaction products are likely to be amorphous as indicated by the halo in the figure.

Table 1. Geometrical characteristics of sealant droplets at the joint different temperatures

Exposure temperature, °C	Droplet height, mm	Reaction layer thickness, mm	Wetting angle, deg
$CaO–SiO_2–B_2O_3$ at Crofer 22 APU steel			
850	5.60	0.10	72
900	5.50	0.30	67
925	4.75	0.45	58
950	2.15	0.6	30
Schott 394 at Crofer 22 APU steel			
950	5.50	–	70
$CaO–SiO_2–B_2O_3$ at ZrO_2-electrolytee			
850	5.55	–	66
900	5.40	–	61
925	4.45	–	50
950	1.95	–	25
Schott 394 at ZrO_2-electrolyte			
950	5.50	–	63

The X-ray diffraction analysis revealed no iron- or chromium-containing crystal phase (the Crofer 22 APU steel basic components) in the blue area. However, the blue color in itself may be connected with the presence of Cr^{3+} ions in the sealant's contacting area. Hence, one can conclude that the amorphous phase formed in the interaction of boron oxide and the steel plate components, to the least. It goes without saying that other sealant components can also contribute to the amorphous phase formation.

To evaluate the sealant and Crofer 22 APU steel thermomechanical compatibility, we cut off rectangular samples from the sealant after its thermal treatment at 950°C. We succeeded in the samples' preparation only of the unreacted sealant area because the reaction zone was too thin (~300 μm). In the SOFC hermitization, the sealant layer thickness comes to about 300 μm, therefore, its composition approaches that of the reaction zone observed in this work. However, the dilatometric data obtained in the sealant zone not contacting the steel (Fig. 3), can give an information, even if approximate one, on the sealant's CTE in the reaction zone because of the closeness of their phase composition.

It is to be noted that the data presented in Fig. 3 are obtained for the sealant after its thermal treatment and do not illustrate any properties of the initial glass. Instead, it reflects the sealant properties after the hermitization procedure. We believe this data being more important for the evaluation of the sealant and steel

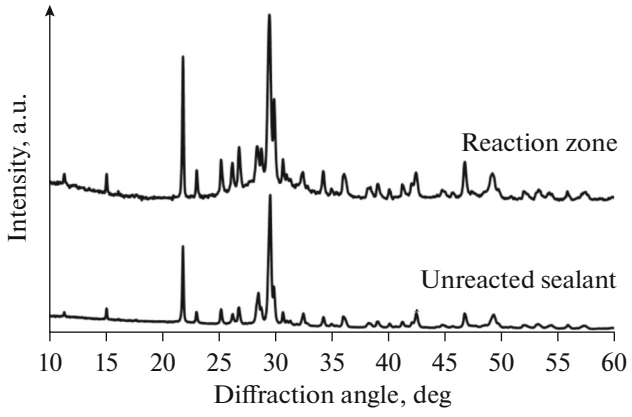

Fig. 2. X-ray diffraction patterns of post-thermal-treated (950°C) sealant.

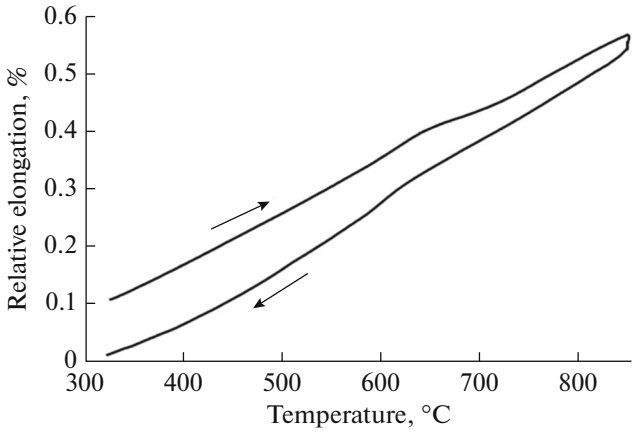

Fig. 3. Dilatometric curve of the studied sealant upon exposure at 950°C for 1 h.

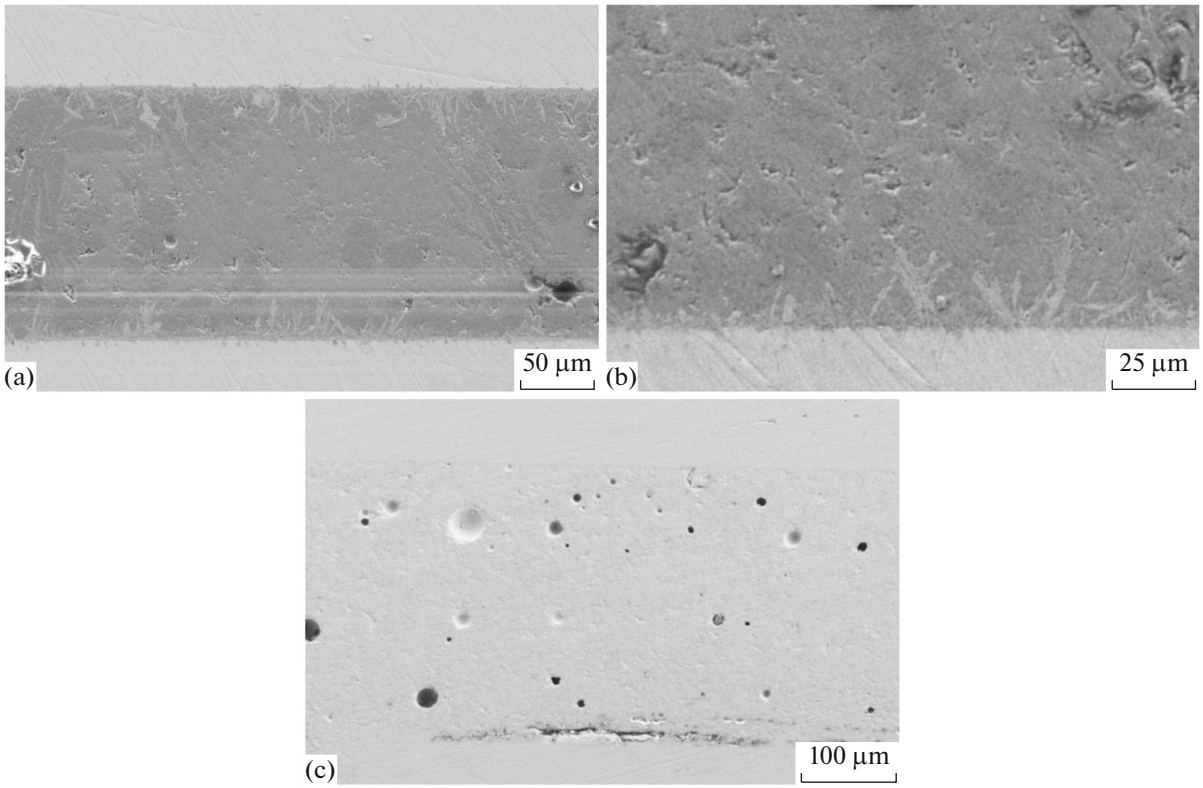

Fig. 4. SEM-images of the steel–sealant joint upon thermal treatment at 950°C for 1 h. The sealant composition: 33 mol % CaO, 21 mol % B_2O_3, 46 mol % SiO_2 (a, b), commercial Schott sealant 394 (c).

plate thermomechanical compatibility. The sealant mean CTE over the 400–850°C temperature range is $(8.9 \pm 0.3) \times 10^{-6}$ 1/K, which is lower than that of the Crofer 22 APU steel ($(11–12) \times 10^{-6}$ at 800–900°C) and ZrO_2-electrolyte ($(10.5–11) \times 10^{-6}$ 1/K). However, this value is close to the Schott 394 glass CTE: 8.6×10^{-6} 1/K. This allows supposing that the obtained sealant with the CTE of 8.9×10^{-6} 1/K is thermomechanically compatible with the Crofer 22 APU steel and the zirconia-based electrolytes.

In Fig. 4 we presented SEM-images of the cross-section of the steel/sealant joint. Figures 4a and 4b correspond to the joint involving the $CaO–SiO_2–B_2O_3$ sealant. We see that a sealant-to-steel chemical reaction zone has formed at the interface. It consisted of elongated crystal forms with preferred orientation perpendicular to the interface. The continuous interaction zone can be observed over the entire sealant/steel surface. A few samples were exposed to the SOFC operational temperature (850°C) for 100 h, to examine the reaction zone stability. The SEM-images of the samples right after the thermal treatment and after the ageing practically do not differ from each other. Therefore, it can be said that the structure formed at the interface is stable at the SOFC operational temperature.

In the Schott 394-containing sample the interaction area is poorly pronounced, as we see from Fig. 4c. In the SEM-image of the joint with the Schott 394 sealant we see areas with the sealant delamination from the steel (the central area at the Fig. 4c top part). The delamination is possible because of poor adhesion in combination with thermal strains at the surface.

To performe the EDX-analysis of the sealant/steel joint, we used joints exposed at 940°C for 3 h. The prolonged thermal treatment is necessary to broaden the area of the sealant–steel interaction and facilitate the experiment al data sampling. The prolonged exposure at higher temperature leads to the reaction zone intense growth with the dendrite penetration deeply into the sealant layer. In Fig. 5 we marked the points at which the material elemental composition was investigated at the sealant/steel joint cross-section. In Table 2 we give data on the elements' content. It is to be noted that the EDX method does not allow determining boron; therefore, the boron is not included in Table 2.

The gray area (point 1 in Fig. 5) predominantly contains Ca, Si, and O, with small admixtures of Cr and Fe. By reference to the Ca/Si and Ca/O ratios, the elemental composition in point 1 cannot be described as a mixture of exclusively $CaSiO_3$ and SiO_2. This points to the presence of calcium borate phase in the

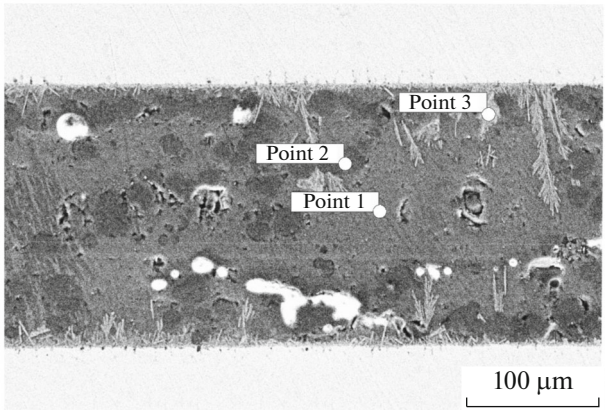

Fig. 5. SEM-microphotograph of the area in which EDX-measurements were done.

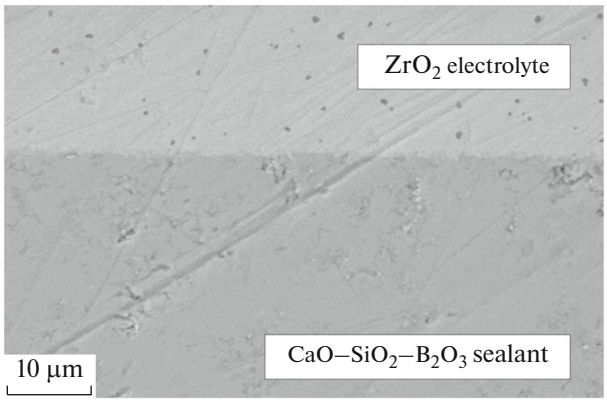

Fig. 6. SEM-image of the sealant/ZrO_2-based electrolyte interface upon exposure at 950°C.

point 1 area. The black area (point 2) demonstrates the presence of nearly pure SiO_2 with small admixture of $CaSiO_3$. The formation of a silica separate area points to its separate crystallization from the joint's amorphous phase. The outgrowths at the interface (point 3) contained quite an amount of Cr and Si, and somewhat of Ca. This shows that at the sealant/steel surface the sealant predominantly interacts with Cr. The molar fraction ratios Cr/Si and Cr/Ca allow supposing with confidence that the reaction product contains quite an amount of boron. This is in good agreement with the XRD data obtained in the reaction zone.

In Fig. 6 we show SEM-microphotographs of the sealant/electrolyte interface obtained upon the heating of the steel/sealant/electrolyte joint up to 940°C with further keeping at this temperature for 3 h. The boundary between the two materials is dense, without splits and delamination. This points to the sealant good adhesion to the solid electrolyte surface and to the closeness of the coefficients of temperature expansion of the studied sealant and ZrO_2-electrolyte. At the same time, we did not observe any pronounced reaction zone formation at the sealant/electrolyte interface. This is connected with the mutual reactivity of our sealant and the ZrO_2-electrolyte.

Table 2. Elemental composition in points shown in Fig. 6

Atom	Content, mol %		
	point 1	point 2	point 3
Si	11.1	33.0	13.0
Ca	22.2	0.7	1.8
O	65.7	66.0	58.2
Cr	0.6	0.1	26.7
Fe	0.4	0.2	0.3

CONCLUSIONS

The sealant comprising 33 mol % CaO, 21 mol % B_2O_3, and 46 mol % SiO_2 can be used in the hermitization of the SOFC by operating near the temperature of 850°C. It has good adhesion to the surfaces of the Crofer 22 APU steel and the ZrO_2-based electrolytes (the basic electrolyte in the solid oxide fuel cells). The studied sealant has the CTE of 8.9×10^{-6} 1/K, comparable with that of commercial sealants, which makes it thermomechanically compatible with the Crofer 22 APU steel and the ZrO_2-based electrolytes. The SEM-images of the sealant/steel interface showed that the interaction between the components provided a strong adhesion at the interface. A short-term ageing at the operational temperature of 850°C for 100 h does not change the interface morphology any significantly, which confirmed the interface stability. The SEM-images also demonstrated a good wettability and strong adhesion of the studied sealant to the ZrO_2-electrolyte surface, which allows thinking of the studied sealant as a material for the first-generation solid oxide fuel cells with the ZrO_2-electrolytes.

However, notably, the 100-h-exposure gives but a pre-information on the sealant/steel-interface and the stability of the sealant per se. Further, longer-exposure experiments are required. Of special interest is the sealant stability in humid atmosphere at the operational temperature, as well as experiments concerning the long-term stability of the SOFCs hermitized with the sealant of the studied composition. Such experiments must allow evaluating the effect of the boron oxide content on the electrode poisoning and investigating the stability of the sealant's dielectric and thermomechanical properties.

FUNDING

This work was supported in part by the grant of President of RF, project no. MK-3060.2022.1.2 (the sealant

preparation and temperature studies), in part by the Russian Science Foundation, grant no. 17-79-30071 P (the microstructure and phase composition study).

CONFLICT OF INTEREST

The authors of this work declare that they have no conflict of interest.

REFERENCES

1. Laosiripojana, N., Wiyaratn, W., Kiatkittipong, W., Arpornwichanop, A., Soottitantawat, P., and Assabumrungrat, S., Reviews on solid oxide fuel cell technology, *Eng. J.*, 2009, vol. 13, p. 65.
2. Shao, Z. and Tadé, M.O., *Intermediate-Temperature Solid Oxide Fuel Cells*, Springer, 2016.
3. Kaur, G., *Intermediate Temperature Solid Oxide Fuel Cells: Electrolytes, Electrodes and Interconnects*, Elsevier Science, 2019.
4. Sing, R. Sealing technology for solid oxide fuel cells (SOFC), *Int. J. Appl. Ceram. Technol.*, 2007, vol. 4, p. 134.
5. Lessing, P.A., A review of sealing technologies applicable to solid oxide electrolysis cells, *J. Mater. Sci.*, 2007, vol. 42, p. 3465.
6. Tietz, F., Thermal expansion of SOFC materials, *Ionics,* 1999, vol. 5, p. 129.
7. Singh, K. and Walia, T., Review on silicate and borosilicate-based glass sealants and their interaction with components of solid oxide fuel cell, *Int. J. Energy Res.*, 2021, vol. 45, p. 20559.
8. Ghosh, S., Kundu, P., Das Sharma, A., Basu, R.N., and Maiti, H.S., Microstructure and property evaluation of barium aluminosilicate glass–ceramic sealant for anode-supported solid oxide fuel cell, *J. Eur. Ceram. Soc.*, 2008, vol. 28, p. 69.
9. Fergus, J.W., Sealants for solid oxide fuel cells, *J. Power Sources*, 2005, vol. 147, p. 46.
10. Sohn, S.-B., Choi, S.-Y., Kim, G.-H., Song, H.-S., and Kim, G.-D., Stable sealing glass for planar solid oxide fuel cell, *J. Non. Cryst. Solids,* 2002, vol. 297, p. 103.
11. Meinhardt, K.D., Kim, D.-S., Chou, Y.-S., and Weil, K.S., Synthesis and properties of a barium aluminosilicate solid oxide fuel cell glass–ceramic sealant, *J. Power Sources*, 2008, vol. 182, p. 188.
12. Kermani, P.S., Ghatee, M., and Yazdani, A., Synthesis and Characterization of Barium Aluminosilicate Glass as the Sealant for Solid Oxide Fuel Cell Application, *Adv. Ceram. Prog.*, 2020, vol. 6, p. 25.
13. Puig, J., Ansart, F., Lenormand, P., Antoine, L., and Dailly, J., Sol-gel synthesis and characterization of barium (magnesium) aluminosilicate glass sealants for solid oxide fuel cells, *J. Non. Cryst. Solids*, 2011, vol. 357, p. 3490.
14. Reddy, A.A., Tulyaganov, D.U., Pascual, M.J., Kharton, V.V., Tsipis, E.V., Kolotygin, V.A., and Ferreira, J.M.F., Diopside–Ba disilicate glass–ceramic sealants for SOFCs: Enhanced adhesion and thermal stability by Sr for Ca substitution, *Int. J. Hydrogen Energy*, 2013, vol. 38, p. 3073
15. Reddy, A.A., Tulyaganov, D.U., Goel, A., Pascual, M.J., Kharton, V.V., Tsipis, E.V., and Ferreira, J.M.F., Diopside—Mg orthosilicate and diopside—Ba disilicate glass–ceramics for sealing applications in SOFC: Sintering and chemical interactions studies, *Int. J. Hydrogen Energy*, 2012, vol. 37, p. 12528.
16. Xie, J., Hao, W., and Wang, F., The analysis of interfacial thermal stresses of solid oxide fuel cell applied for submarine power, *Int. J. Energy Res.,* 2018, vol. 42, p. 2010.
17. Yan, T., Zhang, W., Mao, H., Chen, X., and Bai, S., The effect of CaO/SiO_2 and B_2O_3 on the sintering contraction behaviors of $CaO–B_2O_3SiO_2$ glass-ceramics, *Int. J. Mod. Phys. B*, 2019, vol. 33, p. 1950070.
18. Veron, E., Garaga, M.N., Pelloquin, D., Cadars, S., Suchomel, M., Suard, E., Massiot, D., Montouillout, V., Matzen, G., and Allix, M., Synthesis and structure determination of $CaSi_{1/3}B_{2/3}O_{8/3}$: a new calcium borosilicate, *Inorg. Chem.*, 2013, vol. 52, p. 4250.
19. Dai, B., Zhu, H., Zhou, H., Xu, G., and Yue, Z., Sintering, crystallization and dielectric properties of $CaO–B_2O_3–SiO_2$ system glass ceramics, *J. Cent. South Univ.*, 2012, vol. 19, p. 2101.
20. Chang, C.-R. and Jean, J.-H., Crystallization kinetics and mechanism of low-dielectric, low-temperature, cofirable $CaO-B_2O_3-SiO_2$ glass-ceramics, *J. Amer. Ceram. Soc.*, 1999, vol. 82, p. 1725.
21. Chiang, C.-C., Wang, S.-F., Wang, Y.-R., and Wei, W.-C.J., Densification and microwave dielectric properties of $CaO–B_2O_3–SiO_2$ system glass–ceramics, *Ceram. Intern.*, 2008, vol. 34, p. 599.
22. Shao, H., Wang, T., and Zhang, Q., Preparation and properties of $CaO–SiO_2–B_2O_3$ glass-ceramic at low temperature, *J. Alloys Compd.*, 2009, vol. 484, p. 2.
23. Zhu, H., Liu, M., Zhou, H., Li, L., and Lv, A., Study on properties of $CaO–SiO_2–B_2O_3$ system glass-ceramic, *Mater. Res. Bull.*, 2007, vol. 42, p. 1137.
24. Rodríguez-López, S., Haanappel, V.A.C., Durán, A., Muñoz, F., Mather, G.C., Pascual, M.J., and Gross-Barsnick, S.M., Glass–ceramic seals in the system $MgO–BaO–B_2O_3–SiO_2$ operating under simulated SOFC conditions, *Int. J. Hydrogen Energy*, 2016, vol. 41, p. 15335.
25. Zhang, T., Fahrenholtz, W.G., Reis, S.T., and Brow, R.K., Borate volatility from SOFC sealing glasses, *J. Amer. Ceram. Soc.*, 2008, vol. 91, p. 2564.
26. Inoue, H., Aoki, N., and Yasui, I., Molecular dynamics simulation of the structure of borate glasses, *J. Amer. Ceram. Soc.*, 1987, vol. 70, p. 622.
27. Henderson, G.S., A Si K-edge EXAFS/XANES study of sodium silicate glasses, *J. Non. Cryst. Solids*, 1995, vol. 183, p. 43.
28. Mastelaro, V.R., Zanotto, E.D., Lequeux, N., and Cortès, R., Relationship between short-range order and ease of nucleation in $Na_2Ca_2Si_3O_9$, $CaSiO_3$ and $PbSiO_3$ glasses, *J. Non. Cryst. Solids*, 2000, vol. 262, p. 191.

Translated by Yu. Pleskov